Swirling flow in model of large two-stroke diesel engine

Ingvorsen, Kristian Mark; Meyer, Knud Erik; Schnipper, Teis; Walther, Jens Honore; Mayer, Stefan

Published in:
Proceedings of 16th International Symposium on Applications of Laser Techniques to Fluid Mechanics

Publication date:
2012

Swirling flow in model of large two-stroke diesel engine

Kristian M. Ingvorsen[1], Knud Erik Meyer[1,*], Teis Schnipper[1], Jens H. Walther[1,2], Stefan Mayer[3]

1: Department of Mechanical Engineering, Technical University of Denmark, Lyngby, Denmark
2: Computational Science and Engineering Laboratory, ETH Zürich, Zürich, Switzerland
3: MAN Diesel & Turbo, Copenhagen, Denmark
* correspondent author: kem@mek.dtu.dk

Abstract A scale model of a simplified cylinder in a uniflow scavenged large two-stroke marine diesel engine is constructed to investigate the scavenging process. Angled ports near the bottom of the cylinder liner are uncovered as the piston reaches the bottom dead center. Fresh air enters through the ports forcing the gas in the cylinder to leave through an exhaust valve located in the cylinder head. The scavenging flow is a transient (opening/closing ports) confined port-generated turbulent swirl flow, with complex phenomena such as central recirculation zones, vortex breakdown and vortex precession. The model has a transparent cylinder five diameters long and is fitted with a static valve with a simplified geometry. The piston motion is controlled by a linear motor. The flow in the experiment has a Reynolds number of 50000 based on cylinder diameter and bulk velocity. Stereoscopic Particle Image Velocimetry (PIV) is used to investigate the scavenging flow for cases with both static and moving piston. Measurements are carried out for several cross-sectional planes covering the majority of the cylinder length. The effect of swirl intensity is investigated using four different port angles going from 0 – 30 degree. Although the flow has a relatively low swirl number of around 0.4, a central recirculation zone is observed indicating a vortex breakdown. The steady flow is also analyzed with Proper Orthogonal Decomposition (POD). The analysis reveals systematic variations in the shape and location of the vortex core. Transient measurements using phase-locked PIV are carried out with moving piston. The transient measurements reveal a violent change in flow topology as a central recirculation zone is rapidly formed, resulting in a change from large positive to negative velocities of the axial component.

1. Introduction

Large two-stroke uniflow marine diesel engines are the de-facto standard technology for the propulsion of large commercial vessels, with thermal engine efficiencies being close to 50%. A key process for this type of engine is the scavenging process (Schweitzer, 1949). In a uniflow scavenged engine, scavenge ports located in the lower part of the cylinder liner are uncovered by the piston as it reaches bottom dead center (BDC). When the scavenging ports are uncovered by the piston, compressed air enters through the ports filling the cylinder for the next engine cycle. The introduction of fresh air forces the exhaust gases out through the exhaust valve located in the cylinder head. In order to stabilize the scavenge process and later to enhance mixing of air and injected fuel, the ports are cut at an angle with respect to the local radius to create a swirling flow. The uniflow scavenging process is thus characterized by a transient (opening/closing ports) confined port-generated turbulent swirl flow, with complex phenomena such as central recirculation zones, vortex break down and vortex precession.

Understanding of this confined port-generated turbulent swirl flow is crucial for the optimization of both the scavenge and combustion process. Only few experimental investigations are reported in the literature (see review in Heywood & Sher, 1999) and the majority of these are made in models with strongly simplified static geometries. The early work was based on visualizations (Ferro, 1958), pitot measurements (Percival, 1955) and hotwire measurements (Sher *et al*, 1991). Only few

investigations have been carried out using non-intrusive optical techniques such as Laser Doppler Anemometry (Sung & Patterson 1982, Nakagawa *et al* 1990) and Particle Image Velocimetry (Nino *et al*, 1993).

A larger amount of work exists for guide vane generated swirl flows (e.g. Escudier, 1982 and Mattner, 2002). In a pre-study of the current work Haider *et al* (2012) carried out Stereoscopic PIV measurements for a static setup with guide vane generated swirl. Large Eddy Simulations made for the same geometry was carried out by Obeidat *et al* (2012) and showed good agreement. In the present work a new experimental model is created, well suited for optical measurement. The model extends the work from Haider *et al* (2012) by including the effects of scavenge ports, a static exhaust valve and a movable piston.

The purpose of the study is to describe the flow phenomena occurring during the scavenging process and to provide data that can be used for validation of computer models. Detailed stereoscopic PIV measurements and POD analysis are presented for the static geometry, and the effect of swirl intensity is investigated by varying the port angle. Furthermore, preliminary investigations are presented showing the effect of port opening/closing using a moving piston. The flow in the moving geometry is characterized using phase-locked PIV. The data from the steady flow measurement can be obtained by contacting the correspondent author.

2. Experimental set-up

For the study, a scaled model of a simplified engine cylinder has been constructed, see figure 1. The model has a movable piston driven by a linear motor. The cylinder has an inner diameter of D = 190 mm and is made of glass of good optical quality. With the piston at bottom dead center (BDC), the length of the cylinder is five diameters. The port section consists of 30 equally spaced ports. Each port is a 15 mm slit milled into the cylinder wall with a height (in axial direction) of 76 mm. The top and bottom (maximum/minimum axial position) of the ports are round with a radius of 7.5 mm. The outer diameter of the port section is 228 mm. Four different port sections with different port angles are used. The port angle is the angle between the slit wall direction and radial direction measured mid between slit walls at the inner cylinder wall. The four port angles are 0°, 10°, 20° and 30°. The flow is guided to the ports by two parallel discs with separation equal to the port height and a diameter of 600 mm. The piston has a flat surface and has Teflon seals held towards the glass cylinder by small springs. Experiments are performed using air at room temperature and atmospheric pressure.

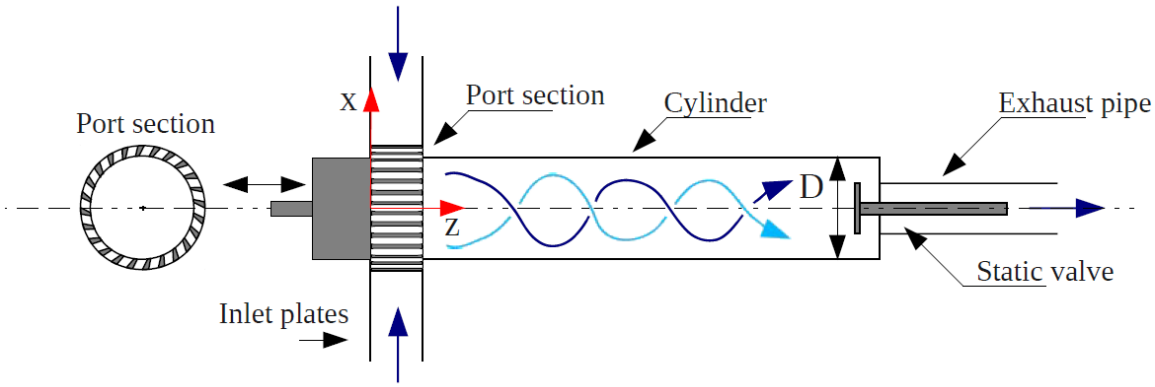

Figure 1 – Sketches of experimental setup.

At the exit of the cylinder is an abrupt change of diameter to an exhaust pipe with a diameter of 95 mm. A simplified exhaust valve is placed at the inlet to the exhaust pipe. This valve consist of a disc (thickness 3.8 mm, diameter 95 mm) mounted on a circular rod (diameter 24 mm, length 255 mm). The valve opening, i.e., the distance between the disc and the cylinder top wall is 28.5 mm.The exhaust pipe has a length of 410 mm and ends in a large cylindrical receiver (diameter 316 mm, length 1.3 m). This receiver is connected to a frequency controlled centrifugal fan. For steady flow measurements (no piston movement) the fan is connected an orifice flow meter.

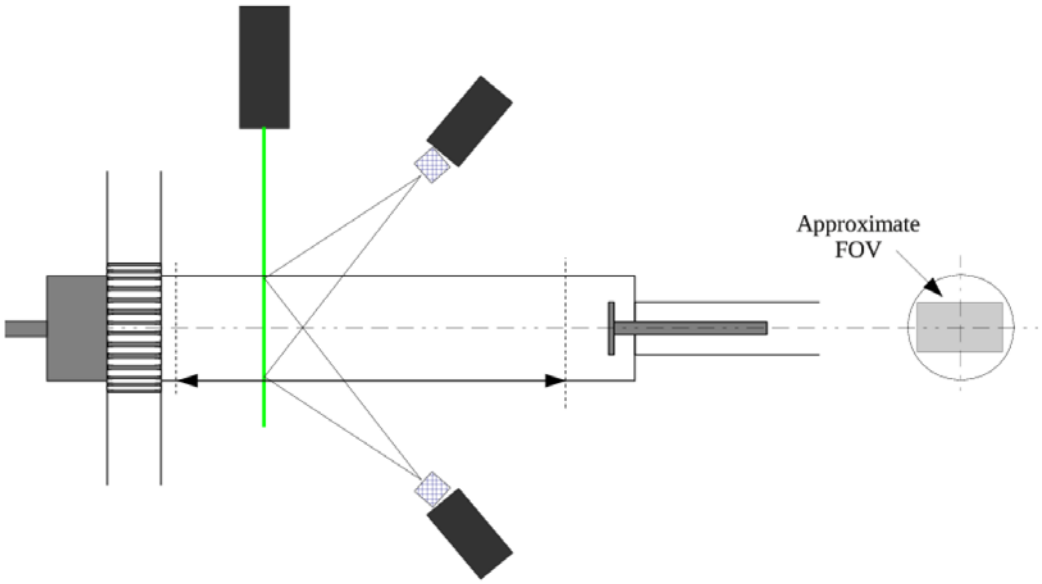

Figure 2 – PIV setup. Arrow on cylinder indicates range of axial positions.

Measurements of the flow field are made with stereoscopic Particle Image Velocimetry (PIV) using two Dantec Hisense II cameras (1344 by 1024 pixels) fitted with lenses (focal length 60 mm) and Scheimpflug mounts, see figure 2. A 200 mJ double pulsed Nd:YAG laser is used to illuminate the flow in a light sheet perpendicular to the cylinder axis. One camera is in forwards scatter mode and the one camera is in backward scatter using F-numbers of 11 and 8, respectively. The cameras and the laser are mounted on a large traversing system aligned with the cylinder axis. This allows measurements at several axial positions using the same calibration. The recorded particle images are processed with Dantec Dynamic studio ver. 3.3 using a three-step adaptive correlation with final interrogation windows of 32 by 32 pixels. The resulting data spacing is about 0.01D. A disparity correction is carried out in order to correct small misalignments between calibration target and light sheet.

The flow rig is placed in a large tent where the ambient air is seeded with DEHS particles (1-2 µm diameter) created with a Laskin nozzle. The flow under steady conditions gives a nominal mean velocity in the cylinder of W_b=4 m/s corresponding to a Reynolds number of Re=50.000 based W_b and D.

Two types of measurement are made with the setup. Steady flow measurements are done with the piston fixed at the BDC (fully open ports) and each measurement series consist of 1000 samples recorded at 6 Hz. Transient measurements are done with a moving piston with each measurement series consisting of a 100 samples(one sample per cycle). The statistical uncertainty is thus larger than for the steady measurements. For the transient measurements the orifice flow meter is decoupled from the fan to reduce flow inertia. A measurement of the pressure difference between the cylinder top and the valve rod showed good correlation with the flow rate at steady flow condition. This pressure measurement is used to set the fan speed for transient measurements.

3. Swirl number

The degree of swirl in a flow can be quantified by the swirl number *S*. Several definitions exist but the most common (Gupta *et al*, 1984, Alekseenko *et al* 2007) is given by

$$S \equiv \frac{2F_{\theta,z}}{F_{z,z}D},$$

where $F_{\theta,z}$ is the flux of angular momentum and $F_{z,z}$ is the flux of axial momentum in the flow direction (axial direction). *D* is the geometrical scale, in this case the cylinder diameter. The swirl number is not known a priori, as it is a result of the flow physics, however it can be estimated using the design swirl parameter based on the flow geometry. The angular momentum flux $F_{\theta,z}$ can be estimated from the radial flux of angular momentum through the ports,

$$F_{\theta,z} \approx F_{\theta,r} = \rho V_\theta V_r R A_{ports},$$

where ρ is the density, V_θ is the tangential velocity component, V_r is the radial velocity component, *R* is cylinder radius and A_{ports} is the area of the ports. The axial momentum is evaluated as

$$F_{z,z} = \rho W_b{}^2 \frac{\pi}{4} D^2.$$

The swirl number as a function of port angle can be evaluated (see table 1). Gupta *et al* (1984) categorizes swirl in three main classes, very weak swirl $S \leq 0.2$, weak swirl $S \leq 0.4$ and strong swirl $S >\sim 0.6$. From this, the main case in the present study (port angle 20°) has weak swirl.

Port angle	Swirl number *S*
0°	0.00
10°	0.15
20°	0.33
30°	0.56

Table 1 – Estimated swirl numbers

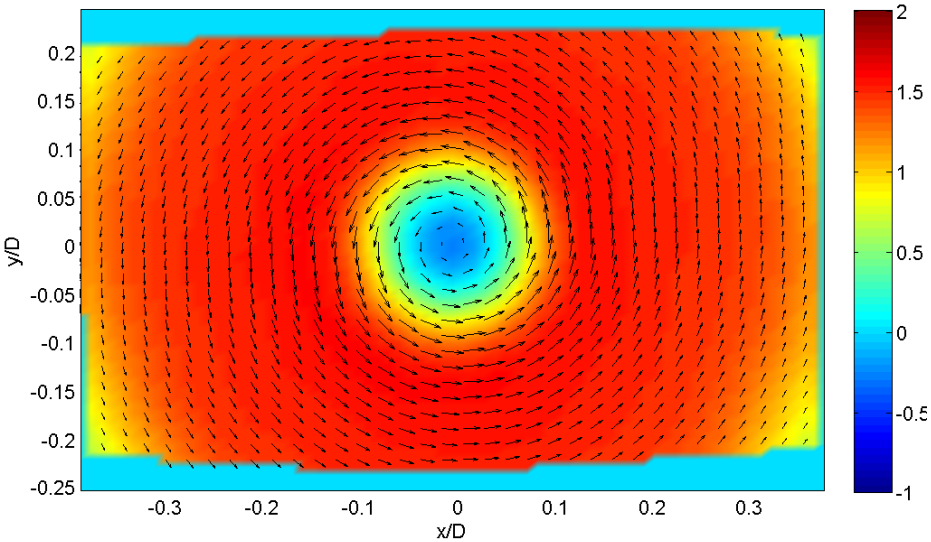

Figure 3 – Mean velocity field at the *z*/*D*=1.00 plane for a port angle of 20°. Color show the out-of-plane mean velocity component V_z / W_b. The region outside the measurement area has been assigned zero velocity. Only every second vector is shown in both directions.

4. Mean velocities for steady flow measurements

Figure 3 shows the mean velocity in the z/D =1.00 plane for a port angle of 20°. The measurements in general cover an almost rectangular region where the corners are relatively close to the cylinder wall. The axial velocity component shows a large region with positive velocity, but has negative velocity near the center corresponding to the central recirculation zone. The in-plane velocities show a swirling flow with large tangential velocities relatively close to the cylinder center corresponding to a concentrated vortex. The mean flow appears to be quite axi-symmetric with the swirl center close to the cylinder axis. The exact swirl center is found by fitting a peak to the in-plane velocity magnitude. In the cross-sectional planes measured, the swirl center is found to be within a few percent of the cylinder diameter from the cylinder center. When the center is found, the velocity field can transformed into polar coordinates where the in-plane position is described by the radius and angle. A fitted curve can be created by binning all points into radial positions and then averaging the velocities. This is shown as a black solid curve in figure 4 for the same axial position as shown in figure 3. We use the symbol r to denote radius in a new coordinate system moved to the estimated swirl center. Gray dots show all data points in the plane. The gray dots coincide well with the fitted curve for $r / D < 0.2$ and they only show a small spread from the fitted curve for larger radius. This demonstrates that the flow is axisymmetric at this axial position.

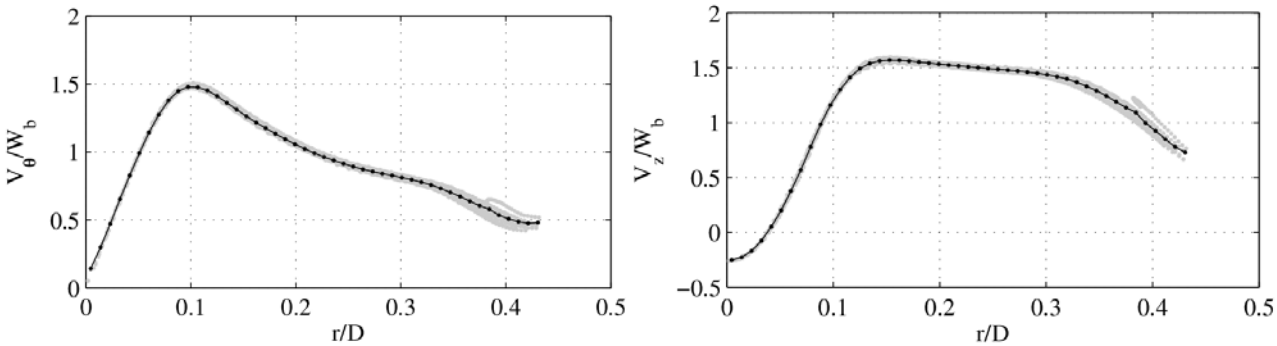

Figure 4 – The mean tangential velocity component V_θ and the mean axial velocity component V_z at the z/D=1.00 position for a port angle of 20°. The gray dots show all data point in the plane and the black curve shows fitted curve found by radial binning.

Profiles of the tangential and axial velocity components are shown for different port angles and axial positions in figure 5. All measurements of the tangential velocity component have a shape similar to a Lamb-Oseen vortex. The vortex core is seen as a sharp linear increase from r=0. The vortex then has a smooth transition to a curve going as $1/r$ for larger values of r. The smallest vortex core is found for port angle 10° at z/D=0.58. For increasing axial position the vortex decays smoothly showing lower tangential velocity and a larger vortex core. Comparing the z/D=0.58 position for the three port angles reveals that larger port angle do create a larger maximum tangential velocity, but a larger port angle also gives a larger vortex core. For the z/D= 0.58 plane all tangential velocities show a sharp decrease near $r/D \approx 0.4$. This is expected to be caused by a separated flow region at the cylinder wall just downstream of the ports.

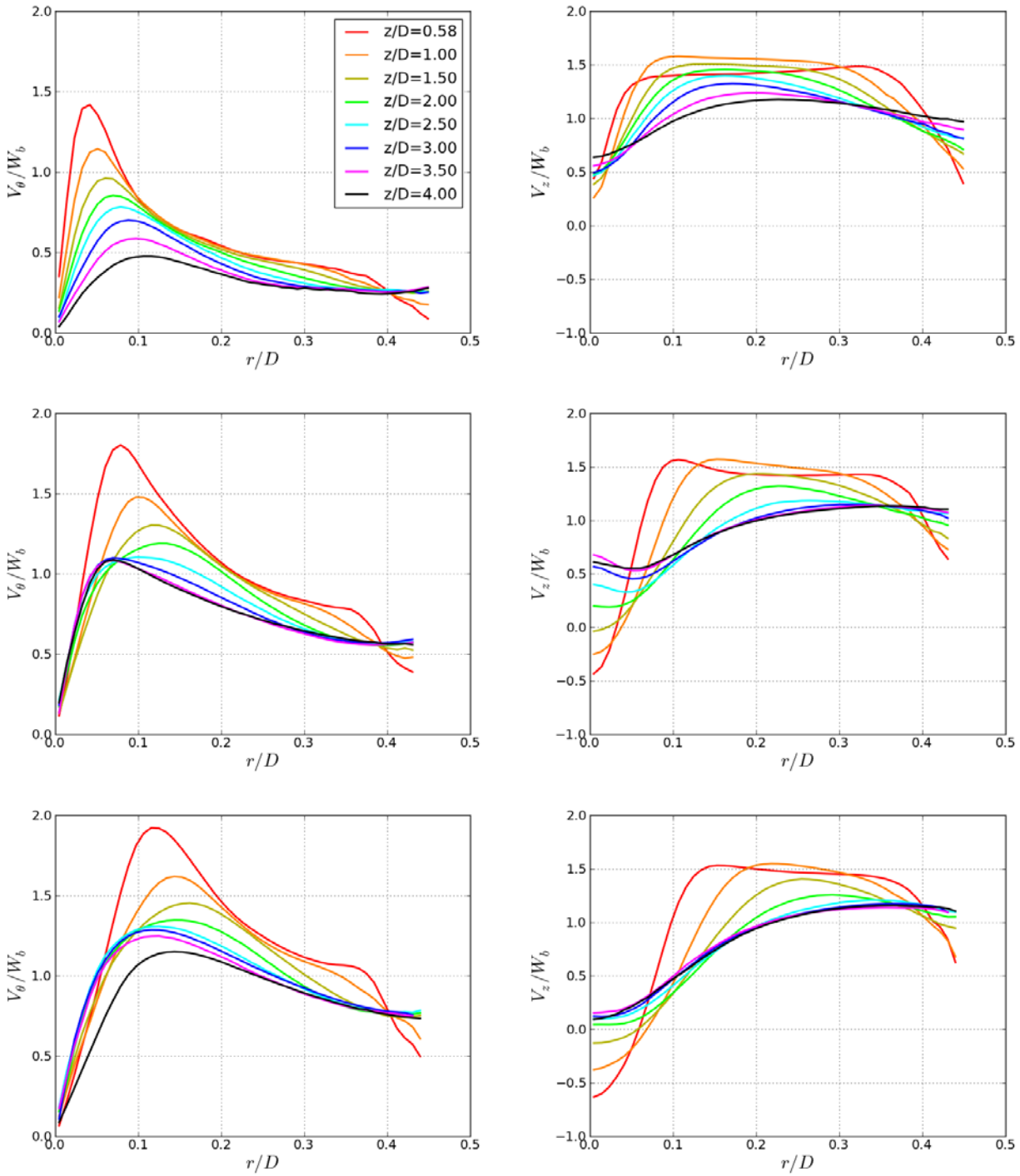

Figure 5 – Profiles of the tangential velocity component V_θ (left column) and the axial velocity component V_z (right column) for three different port angles: 10° (top row), 20° (middle row) and 30°(bottom row).

The axial velocities show a relatively uniform velocity in the main part of the cylinder cross section. The profiles for z/D=0.58 have a clear decrease near the cylinder wall. This is again expected to be caused by the separated region above the ports. All profiles show low velocity in the region of the vortex core. For the 10° port angle, all axial velocities are positive and the lowest value is found for z/D=1.00. For port angles of 20° and 30°, negative axial velocity components are found in the vortex core for positions close to the piston. In both cases the minimum axial component is found

for z/D=0.58, suggesting that even lower axial components can be found closer to the piston. The region with negative axial velocity component can be viewed as a vortex breakdown. For a port angle of 20° the region extents to z/D=1.50 and for a port angle of 30° the region extents to z/D=2.00.

The tangential velocities for port angle of 20° show a similar decay of the vortex core for z/D<2.00 as observed for a port angle of 10°. However, further downstream, the vortex core decreases in size. The axial velocity component also behaves differently for z/D>2.00. The velocity at the center is now a local maximum and the lowest value is found at the edge of the vortex core. This fundamentally changes of the vortex. A likely explanation is that the vortex gets contact with the suction from the exhaust pipe. This is not trivial since the exhaust pipe has the exhaust valve in front of it. This suggests that the vortex core somehow bends around the valve disc and into the exhaust pipe.

For a port angle of 30°, a similar change in the tangential velocity is seen. Two important differences are: (1) the tangential velocity profile close to the valve (z/D=4.00) indicates a new expansion of the vortex core, (2) the axial velocity profiles do not show a new peak at the center.

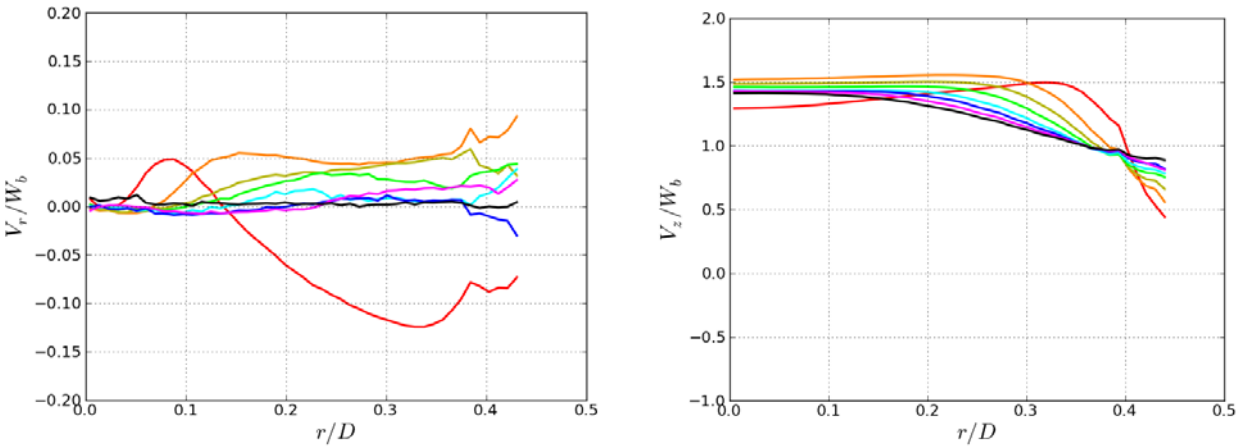

Figure 6 – Profiles of the radial velocity component V_r for a port angle of 20° (left) and of the axial velocity component V_z for a port angle of 0° (right). Se figure 5 for legend.

The radial velocity component for port angle of 20° is shown in figure 6. For the first axial position (z/D=0.58) a modest variation indicates that the turning of the inlet flow from radial direction to axial direction is almost completed at this position. Further downstream the radial velocity component is practically negligible. Figure 6 also shows axial velocity profiles for a port angle of 0°. The profiles show a mostly uniform velocity profile with a decrease of the velocity close to the wall. This boundary layer like decrease of velocity covers quite a large region for more downstream profiles. This suggests that the flow is not close to a fully developed pipe flow within the five diameters length of the cylinder.

5. Analysis of flow dynamics for steady flow measurements

For analysis of the flow dynamics, snapshot Proper Orthogonal Decomposition (POD) analysis is used. The method is described by Meyer *et al* (2007). POD analysis finds “modes” that decompose a snapshots fluctuations from the mean fields in an “optimal” way using eigenvectors of the cross correlation between snapshots. The eigenvalue represents the part of the kinetic energy of

fluctuations from the mean field that a particular mode accounts for. A snapshots can be reconstructed perfectly by multiplying each mode *i* with a corresponding reconstruction coefficient a_i and adding the sum of these products to the mean field. Modes are sorted with respect to energy with the most energetic mode as mode 1. A particular snapshot can therefore often be reconstructed satisfactorily using a few of the first modes.

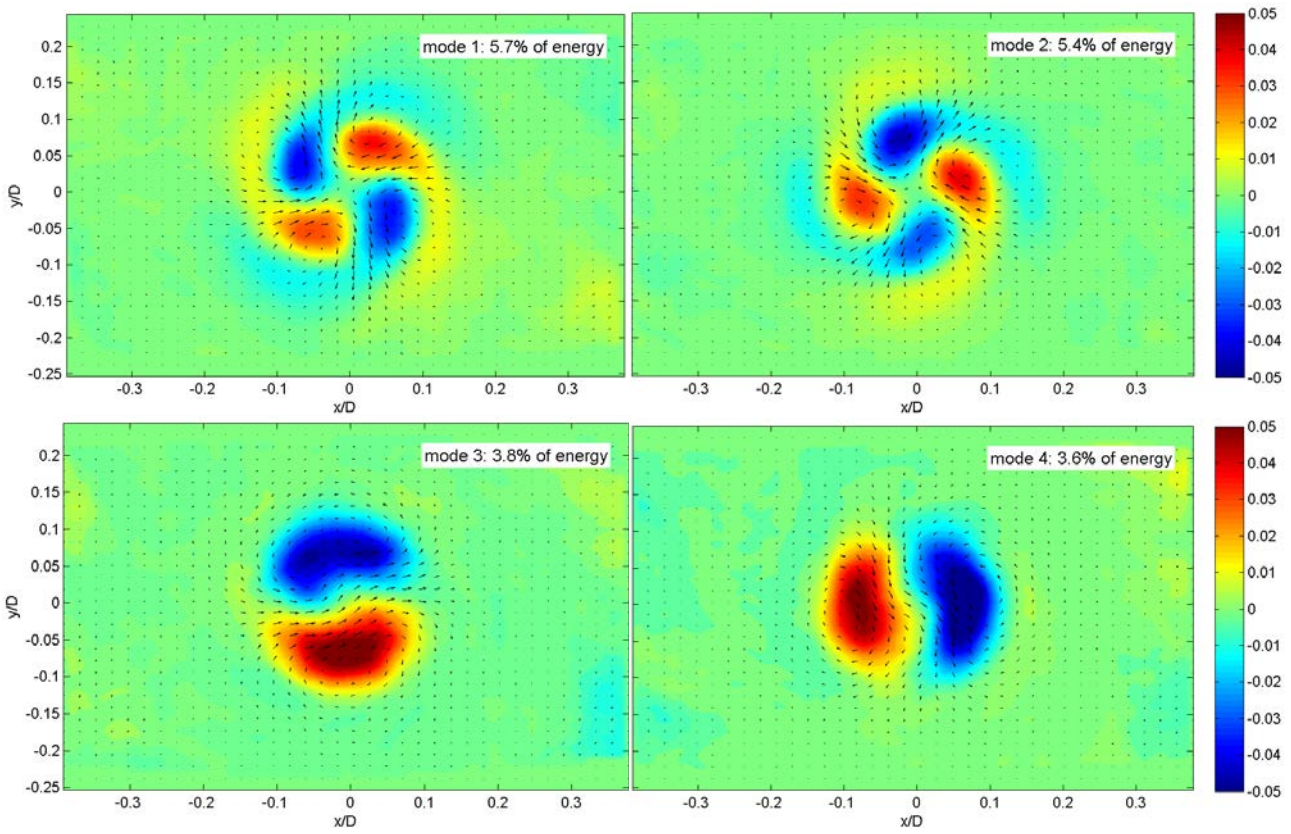

Figure 7 – First four POD modes at z=1.00D plane for port angle of 20°. Color show the out-of-plane component. Only every second vector is shown in both directions.

Figure 7 shows the first POD modes from the z/*D*=1.00 plane for a port angle of 20°. The first two modes represent significant more of the fluctuating kinetic energy (about 5.5% each) than the following modes. Still, the relative energy is relatively low. This is probably because the activity in the modes is confined to a small region, namely the vortex core. Mode 1 has two regions with positive out-of-plane component and two regions with negative out-of-plane component arranged in circular, alternating pattern around the cylinder center. In a polar coordinate system this corresponds to an azimuthal mode with a period of two (*k*=2). Mode 2 is identical to mode 1 rotated 45° or a quarter of an azimuthal wavelength. A linear combination of the two modes (perhaps using a negative coefficient) can create any rotation of the pattern. To interpret the pattern it should be added the mean field shown in figure 3.

This is done in figure 8. A snapshot has been selected based on its reconstruction coefficients a_i. The snapshot has a high value of the first coefficient a_1, but relatively low values of the following coefficients. This gives an impression of the effect of mode 1. The mode causes an elongation of the vortex core. Inspection of the variation of a_1 and a_2 in time shows periods with variation between mode 1 and mode 2 in cosine – sine like relationship. The period time is slightly longer than 0.5 s.
This suggests that the elongated core has regular rotation some of the time. Both the snapshot and the reconstruction show higher axial velocity at the two ends of the elongation. Visualizations made

with smoke and inspected by eye sometimes reveal two streaks of smoke in a spiraling pattern. This could be traces of the high speed regions at the ends of the elongation. Mode 1 and 2 may therefore be associated with a vortex core that has a “twisted tape” shape and that rotates in time.

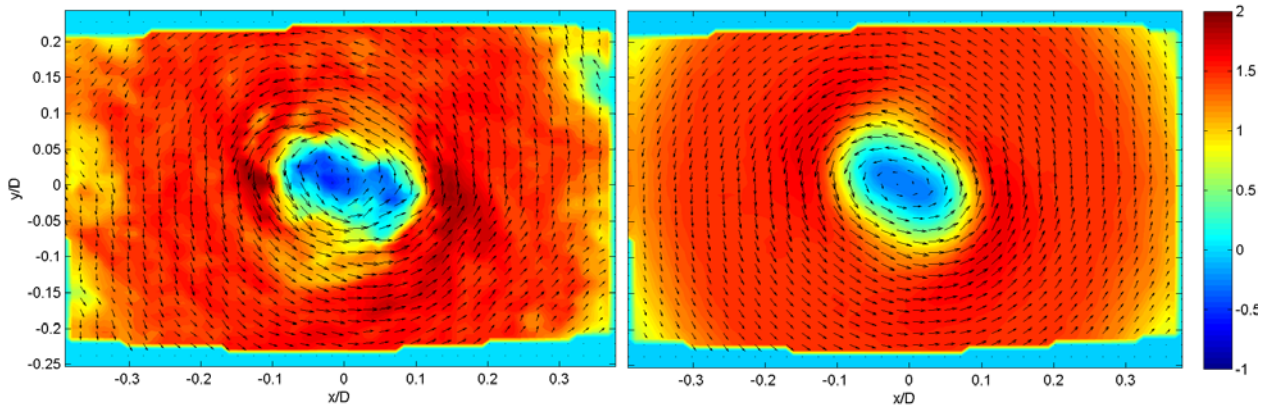

Figure 8 – Snapshot (left) of the flow and the corresponding reconstruction (right) using the first POD mode only. Plots at z=1.00D plane for a port angle of 20°. Colors show the out-of-plane velocity component V_z/W_b. Only every second vector is shown in both directions.

Mode 3 and 4 also represent more relative energy compared to following modes. The modes are again azimuthal modes, but now with a period of one (k=1). Mode 4 is identical to mode 3 rotated 90° or a quarter of an azimuthal wavelength. When mode 3 or mode 4 is added to the mean field, it displaces the vortex core in the y-direction or x-direction, respectively. A linear combination of mode 3 and 4 can reconstruct displacement of the vortex of a few percent of D from the center. This suggests that this type of variation is typical for the flow. Inspection of the variation of a_3 and a_4 in time show both rapid variation and long scale variation. The long scale variation is in the order of 10 s. This suggests that a slight asymmetry are sometimes found with the vortex core slowly precessing around the center.

POD analysis of more downstream positions show that for z/D=1.50, the relative energy of the first mode is almost equal to the following modes, indicating no dominant flow structures. This is the position where the vortex breakdown ends. For following positions, the two first modes are k=1 type modes, but covering a large region of the flow at the center. The relative energy of the first two modes increases with increasing z. The maximum relative energy is found for z/D=3.50 – here mode 1 and 2 together represent a third of the kinetic energy of the velocity fluctuations. This could suggest that the vortex core is precessing to make its way around the valve disc. Systematic variations seem to occur in the reconstruction coefficients, but frequencies are probably too high to resolve.

For a port angle of 30°, the POD analysis is in general similar to the analysis for port angle 20°. More complex vortex core shapes are found in the vortex breakdown region and stronger displacements of the vortex core are found near the exhaust valve. For a port angle of 10°, the POD analysis finds much less systematic variations in the flow. The main finding is small k=1 modes for low values of z.

6. Transient measurements

Phase locked PIV measurements are carried out for a case where the piston is opening and closing the ports. The piston starts at z/D=1.00, opens and closes the ports following a sine curve with a period of T=0.68 s. Having returned to z/D=1.00 the piston goes into standstill mode for 3.00 s

before the cycle is repeated. Using a trigger signal from the servo controller, phase locked PIV measurements can be carried out for arbitrary piston positions.

The bulk velocity during port opening is estimated from the pressure drop between cylinder top and valve rod. The time that the port is (partly) open is called T_{port}. A characteristic scavenge velocity is defined by

$$U_{sc} = \int_0^{T_{port}} W_b d \frac{dt}{T_{port}}$$

The fan speed can then be adjusted so that the Strouhal number for the scavenging process in the model St= fD/U_{sc} matches that of a full scale engine. This corresponds to a scavenged air volume slightly larger than the volume of the cylinder. The used port opening time is $T_{port} = 0.297$ s.

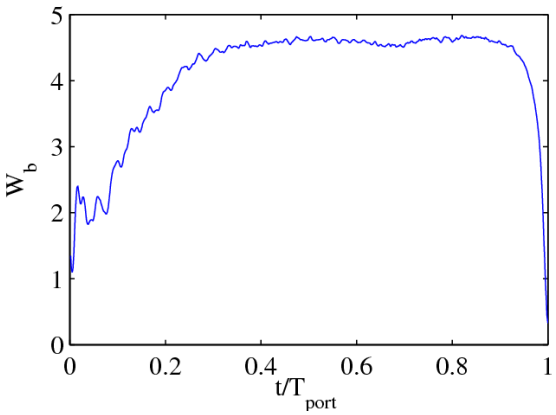

Figure 9 – The phase-averaged bulk velocity W_b (in m/s) in the cylinder estimated from the pressure difference between cylinder top and valve rod.

Figure 9 shows the estimated phase-averaged velocity W_b in the cylinder during the transient measurements. Although the port opening is symmetric, the velocity is not symmetric in time. The applied pressure difference accelerates the flow relatively slowly when the port opens due to inertia of the air. When the port closes, the deceleration of the flow occurs fast.

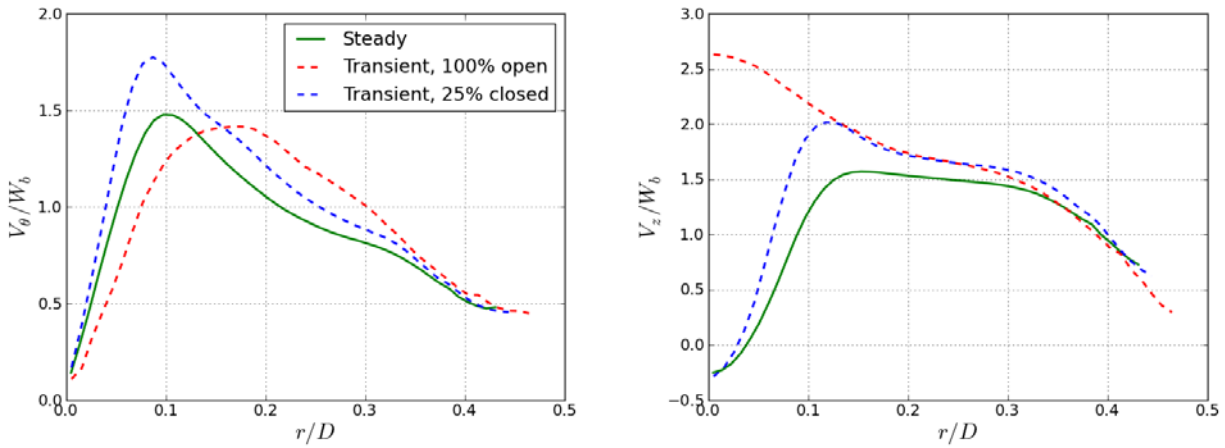

Figure 10 – Transient phase-averaged velocity profiles of tangential velocity component (left) and axial velocity component (right) at z=1.00D plane for a port angle of 20°.

Figure 10 shows two example of phase-averaged velocity profiles at the z/D=1.00 plane for a port angle of 20°. Profiles are measured at BDC (fully open ports) with t/T_{port}=0.5 and a short while later where the ports have become 25% closed (moved 25% of the port height in axial direction) at t/T_{port}=0.752. The two sets of measurements are surprisingly different. At BDC, the central vortex has a relatively large core and maximum axial velocity is found at the center. At 25% closed ports the vortex core is only half the size and the axial velocity at the center is now the minimum velocity. This velocity is negative indicating that a vortex breakdown now is present. The vortex core is smaller than under steady flow conditions, but the negative axial velocity at the center takes the same value.

7. Conclusion

A scale model of a simplified two-stroke diesel engine cylinder has been constructed. It models the flow during the scavenging process in the engine. The model has realistic port geometry and a moving piston controlled by a linear motor. The model has a simplified static exhaust valve. The experiments run at atmospheric pressure and at room temperature. The compression and expansion of gas is therefore not modeled. Both steady (fixed piston, fully open ports) and transient flow measurements (moving piston) are presented. The intake ports have an angle with radial direction and the flow therefore forms a large vortex in the cylinder. Four different port angles were investigated: 0°, 10°, 20° and 30°. Port angles of 20° are used in engines today.

For steady flow measurements, the mean flow is found to be symmetric within a couple of percent of the diameter. For a port angle of 10°, a very strong vortex in found just above the ports (z/D=0.58). This vortex is similar to a Lamb-Oseen vortex. Moving downstream, the vortex decays: the vortex core expands and the maximum tangential velocity decreases. The axial velocity component takes a small value in the vortex core. Outside the vortex core, the axial velocity is relatively constant. For higher port angles (20° and 30°), the vortex core starts less concentrated. The axial velocity component has negative values near the center in the region closest to the piston showing a central recirculation zone. The central recirculation region could be a result of a vortex breakdown. Further downstream, the case with port angle 20° is different from the others: the axial velocity component has a new positive peak at the center. It is expected that the peak is related to the suction from the exhaust pipe, but additional measurement close to the exhaust pipe needs to be performed to clarify this phenomenon.

Dynamic flow structures in the steady flow measurements are analyzed with POD. For a port angle of 20° the analysis show systematic variations in the vortex core relatively close to the piston. The two strongest modes describe an elongation of the vortex core that rotates relatively slowly with the flow. The next two modes describe movement of the vortex core around the center. Regular variation of the reconstruction coefficients indicate that both types of phenomena happen at relatively slow time scale. The POD analysis indicates strong movements of the vortex core near the exhaust valve for the higher port angles. This analysis is promising for a detailed description of flow phenomena. Increasing the image frame rate by reducing image resolution can improve the analysis. Measurements even closer to the exhaust valve will be valuable for understanding of the dynamics here.

The measurements of the transient flow created with a moving piston show qualitative differences. With piston at BDC, the axial velocity component has its maximum at the center. A short while later (piston movement 25% of port height) the phase-averaged axial velocity component now has the minimum value at the center with flow reversal (possible vortex breakdown) and is thus similar to the steady flow conditions. This change happens very rapidly. Transient flow measurement is a

work in progress and more data will be presented at the oral presentation.

Future work will include investigation of the mixing and scavenging of stagnant in-cylinder gas by fresh air from the ports. This will be carried out using Mie-scatter based concentration measurements (Ingvorsen *et al*, 2012). In parallel projects, the flow is simulated using different turbulence models, both Reynolds averaged (RANS) and Large Eddy Simulation (LES). Initial results confirm that the flow is difficult to simulate and that standard models do not give satisfactory results.

Acknowledgement

Financial funding from the Danish Agency for Science Technology and Innovation (Grants No. 09-070608, MAN Diesel & Turbo) is greatly acknowledged.

References

Alekseenko SV, Kuibin PA, Okulov VL (2007) Theory of Concentrated Vortices: An Introduction. Springer-Verlag

Escudier MP, Bornstein J, Maxworthy T (1982) The dynamics of confined vortices, Proceedings of the Royal Society of London, Series A (Mathematical and Physical Sciences), 382, 335 – 360.

Ferro, A. (1958), Investigation by means of models into the scavenging of two-stroke internal combustion engines, The Engineers' Digest, 19, 512–522.

Haider S, Schnipper T, Obeidat A, Meyer KE, Okulov VL, Mayer S, Walther JH (2012), PIV study of the effect of piston position on the in-cylnder swirling flow during the scavenging process in large two-stroke marine diesel engines, Journal of Maritime Science and technology, under review.

Heywood, JB and Sher, E (1999), The two-stroke cycle engine / Its development, operation, and design, Taylor & Francis.

Ingvorsen KM, Meyer KE, Nielsen NF (2011), Planar measurements of velocity and concentration of turbulent mixing in a T-junction, 9th international symposium on particle image velocimetry, Kobe, Japan, July 21-23.

Gupta AK, Lilley DG, Syred N (1984) Swirl Flows. Abacus Press

Mattner TW, Joubert PN, Chong MS (2002), Vortical flow. Part 1. Flow through a constant-diameter pipe, Journal of Fluid Mechanics, 463, 259 – 291.

Meyer, KE, Pedersen JM, Özcan O (2007) A turbulent jet in crossflow analysed with proper orthogonal decomposition. Journal of Fluid Mechanics, 583, 199–227.

Nakagawa H, Kato S, Teteishi M, Adachi T, Tsujimura H, Nakashima M, (1990), JSME International journal, 33, 591 – 598.

Nino E, Gajdeczko BF, Felton PG (1993), Two-Color particle image velocimetry in an egnine with combustion, SAE Transactions, 1273 – 1279.

Obeidat A, Schnipper T, Ingvorsen KM, Haider S, Meyer KE, Mayer S, Walther JH (2012), Large eddy simulations of the influence of piston position on the swirling flow in a model two-stroke diesel engine, International Journal of Numerical Methods for Heat and Fluid Flow, under review.

Percival WH (1955), Method of scavenging analysis for 2-cycle diesel cylinders, Society of Automotive Engineers – Papers. 63, 737 – 751.

Schweitzer PH (1949) Scavenging of two-stroke cycle diesel engines. The Macmillan company.

Sher, E and Hossain, I and Zhang, Q and Winterbone, DE (1991), Calculations and measurements in the cylinder of a two-stroke uniflow-scavenged engine under steady flow conditions, Experimental Thermal and Fluid Science, 4, 418 – 431.

Sung NW and Patterson DJ (1982), Air Motion in a two stroke engine cylinder – the effects of exhaust geometry, SAE Trans, 9, 2534 – 2544.